Assessment of photosensitization performance and stability of host-guest MCM-41 composites from the direct observation of singlet oxygen formation and properties

Tatevik Chilingaryan, Adrien Schlachter, Céline Frochot, B. Habermeyer, Pierre Harvey, Roger Guilard

Assessment of photosensitization performance and stability of host-guest MCM-41 composites from the direct observation of singlet oxygen formation and properties

Tatevik Chilingaryan[a,d,◊], Adrien Schlachter[c], Céline Frochot[d], B. Habermeyer[a,◊], Pierre D. Harvey[c,*], and Roger Guilard[a,b,*,◊]

[a] *PorphyChem - Porphyrin Chemicals & Engineering, 390 rue Charles de Freycinet, ZAC de Beauregard, 21600 Longvic – France.*
[b] *Institut de Chimie Moléculaire de l'Université de Bourgogne, ICMUB, UMR CNRS 6302, Université de Bourgogne Franche-Comté, F-21078, France*
[c] *Département de chimie, Université de Sherbrooke, Sherbrooke, PQ, Canada J1K 2R1*
[d] *CNRS-Université de Lorraine, Laboratoire Réactions et Génie des Procédés (LRGP), 54000 Nancy, France*

Received
Accepted

Dedicated to Prof. Tomás Torres on the occasion of his 70th birthday

ABSTRACT: New heterogeneous porous materials based on 5,10,15,20-(tetraphenyl)porphyrin (H_2TPP), 5,10,15,20-(tetra-N-methyl-4-pyridyl)porphyrin tetrachloride (TMePyP), zinc(II) 5,10,15,20-(tetra-N-methyl-4-pyridyl)porphyrin tetrachloride (ZnTMePyP), 5,10,15,20-(tetra-4-carboxyphenyl)porphyrin (TCPP) and zinc(II) 5,10,15,20-(tetra-4-carboxyphenyl)porphyrin (ZnTCPP) have been incorporated into mesoporous silica MCM-41 from slow diffusion of solutions containing different concentrations of porphyrin chromophores. Successful incorporation of all porphyrins has been confirmed by UV-Vis spectroscopy and TGA. XRD patterns of these silica-based host-guest samples prove that the mesoporous structure of MCM-41 remains unchanged after encapsulation. The characteristic properties of these photosensitizers for singlet oxygen ($^1O_2$(g)) at the solid state/air interface were investigated. Despite the variable amount of encapsulated porphyrin derivatives (based on UV-vis assessment and chemical analysis), the phosphorescence intensity of $^1O_2$(g) peak at 1270 nm remains relatively the same from one composite to the other meaning that the photosensitizers are mainly placed at the surface of the MCM-41 particles.

KEYWORDS: MCM-41, free base and zinc porphyrins, encapsulation, mesoporous materials, singlet oxygen.

◊SPP full member in good standing.
*Correspondence to: Pierre Harvey, e-mail: Pierre.Harvey@USherbrooke.ca, Roger Guilard, e-mail: Roger.Guilard@u-bourgogne.fr

INTRODUCTION

Metal-organic frameworks (MOFs) are tremendously versatile porous materials. The pore sizes may vary from one to several nm [1] and can incorporate organic molecules and complexes of variable sizes for storage purposes [2], capture of toxins [3], separation of molecules [4], space-constrained reactions and catalysis [5], and controlled drug delivery [6], just to name a few. Among guest molecules, thermo-, electro-, and photocatalysts have been commonly incorporated inside MOFs such as MOF-5 [7–13], HKUST-1 [14–17], MIL-101 [18–20], UiO-66 [21–25], and MCM-41[26–29]. MCM-41 materials (Mobil Composition of Matter) are members of the M41S family. Very quickly, since their discovery by Mobil Oil Corporation [30], these materials became an interesting research area and their use started to cover a wide range of applications: drug delivery [31], extraction [32], catalysis [33, 34], and luminescent sensors [35]. It is known that MCM-41 has large pore volumes and surface area [36], which on one hand, renders easier the incorporation of new molecules, and on the other hand has less effect on the electronic structure of the guest complex. One notorious pigment encapsulated as a guest chromophore inside MOF, and MCM-41, is porphyrin free base or its metallated form (porphyrin@MOF). These highly colored porphyrin derivatives are ideal materials for the design of nanosized MOFs exhibiting visible-light-driven photocatalytic reactions and photosensitization [37–41]. It is noteworthy that, to the best of our knowledge, only four earlier investigations concerned the photocatalytic degradation of pesticides and organics by various porphyrin-free bases and metalloporphyrin derivatives immobilized inside MCM-41 matrices [42–45], but the area turned to be surprisingly quiet ever since. In front of these odd observations, five

porphyrin dyes, 5,10,15,20-(tetraphenyl)porphyrin (H_2TPP), 5,10,15,20-(tetra-N-methyl-4-pyridyl)porphyrin tetrachloride (TNMPyP), its zinc derivative (ZnTNMPyP), 5,10,15,20-(tetra-4-carboxyphenyl)porphyrin (TCPP) and its zinc derivative (ZnTCPP) were inserted inside MCM-41 and their ability to photosensitize singlet oxygen, $^1O_2$, was investigated in the solid state and in solution using the $^1O_2$ phosphorescence signal as diagnostic (λ_{emi} = 1270 nm). The codes of these host-guest composites are provided in Figure 1; H_2TPP@MCM-41, TNMPyP@MCM-41, ZnTMPyP@MCM-41, H_2TCPP@MCM-41 and ZnTCPP@MCM-41).

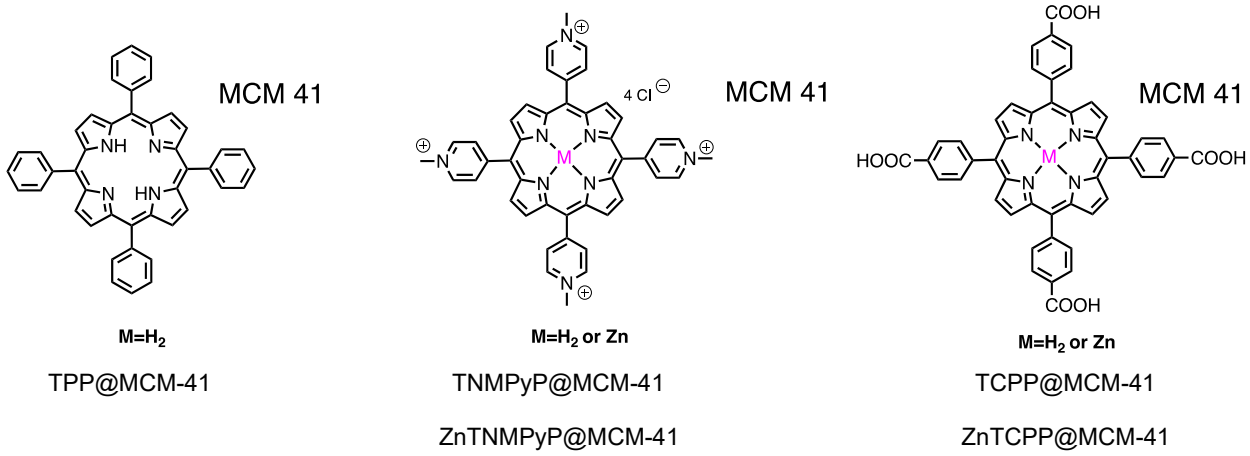

Figure 1. Structures of the host-guest composites.

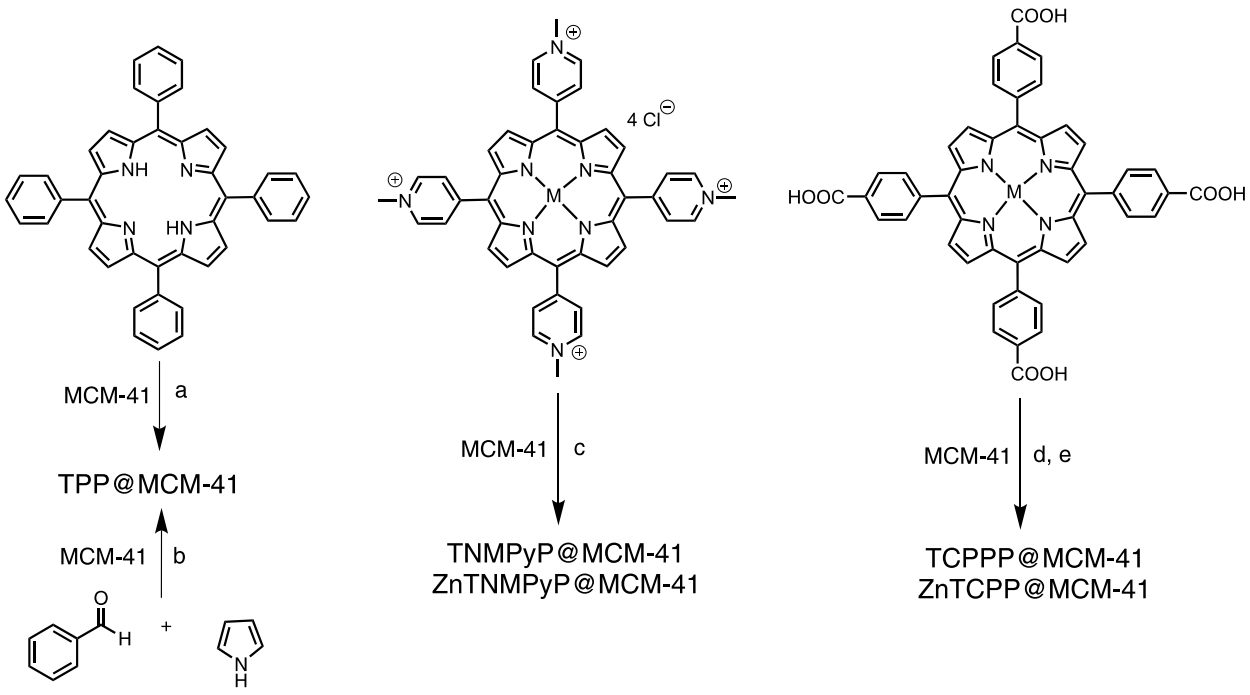

Scheme 1. Synthesis of the host-guest composites: a) CH_2Cl_2, RT, 1hr; b) benzaldehyde, pyrrole, toluene, reflux, 12 hr; c) H_2O, RT, 1 hr; d) DMSO, RT, 1 hr; e) H_2O, RT, 1 hr.

RESULTS AND DISCUSSION

Synthesis

The free base and metal porphyrins have been prepared according to the literature procedures [46, 47], and were incorporated inside mesoporous MCM-41 (Scheme 1). The free base@MCM-41 and metal porphyrin@MCM-41 host-guest composites have been prepared by the addition of a porphyrin solution to an MCM-41 suspension in an appropriate solvent (H_2O, CH_2Cl_2, or DMSO). The synthesis of TPP inside MCM-41 was also performed for the first time and was obtained *via* the direct addition of MCM-41 into the mixture of benzaldehyde, pyrrole, and toluene (Scheme 1). The characterization data of TPP@MCM-41 (below) prepared by the incorporation of TPP in MCM-41 with that synthesized directly inside the pores are found to be identical thus confirming their identities. Successful

incorporation of the porphyrin molecules inside MCM-41 is confirmed by the presence of the same IR peaks of the porphyrins along with the broad signal associated with H-bonded OH groups of MCM-41 in the IR spectra (Supplementary Materials).

Characterization of porous materials

Ultraviolet-Visible Spectroscopy (UV-Vis)

The UV-Vis spectra of TPP and TTP@/MCM-41 in CH_2Cl_2 solution and in the solid state are presented in Figure 2. The spectra of TMPyP, TMPyP@MCM-41, ZnTMPyP, ZnTMPy@/MCM-41, TCPP, TCPP@MCM-41, ZnTCPP, and ZnTCPP@MCM-41 are provided in the Supplementary Materials. The absorption spectrum of TPP exhibits the expected intense Soret band at 416 nm. After immobilization of TPP onto MCM-41, the Soret band shifted from 416 nm to 419 nm (Figure 2a). TNMPyp exhibits a Soret band at 423 nm and ~11 nm red-shift was observed when the porphyrin was incorporated inside MCM-41. The absorption spectrum of ZnTMPyP exhibits a Soret band centered at 436 nm. After porphyrin immobilization in the mesoporous MCM-41, the UV-Vis spectrum of ZnTMPyP@MCM-41 shows a bathochromic shift of 12 nm. Conversely, the Soret band of TCPP (422 nm) and ZnTCPP (420 nm) remains unchanged after their incorporation into MCM-41. All in all, the porphyrin dyes have been successfully incorporated inside MCM-41 as further confirmed by UV-Vis spectroscopy.

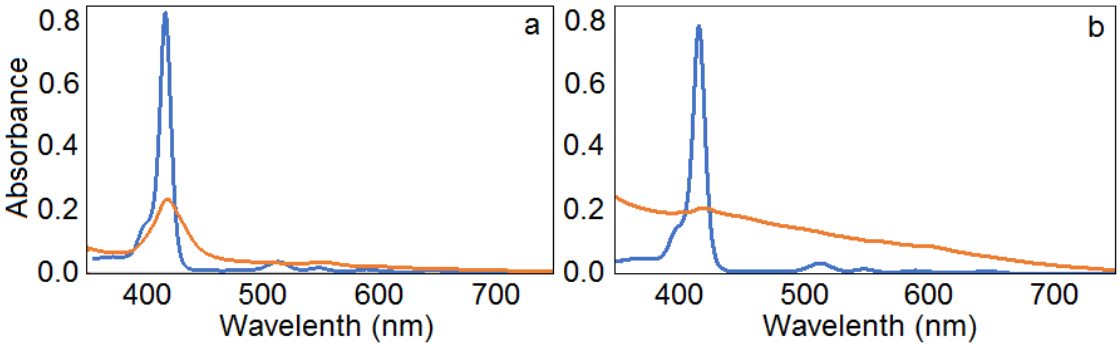

Figure 2. UV-Vis spectra of TPP@MCM-4 (a) and TPP@CM-41 direct synthesis (b) (blue = DCM solution of TPP, orange = DCM suspension of TPP@MCM-41). Note that the baselines of the MCM-41-based composites are not flat due to light scattering.

UV-Vis spectroscopy and the Beer-Lambert law monitoring the Soret band were used to quantify the amount of porphyrin inside the host-guest composites (Table 1). The observations are as follows, first, for an identical amount of porphyrin exposed to MCM-41 in a given solvent for an identical amount of MCM-41 (per 2 mg), the trend is TCPP@MCM-41 < TPP@MCM-41 < TNMPyP@MCM-41 ≤ ZnTCPP@MCM-41 < ZnTNMPyP@MCM-41, and second, for a variation of the number of mg of porphyrin accumulated inside MCM-41 increase with the number of mg exposed to MCM-41 but not proportionally, but rather much less. This latter outcome predictably indicates that the outside pores are filled first and then slow down the entry of the following porphyrin guest. The former trend may reflect the relative affinity of the porphyrin molecules with the mesoporous MCM-41 versus the solvent. This explanation is well exemplified by comparing TCPP (in DMSO) and ZnTCPP (in H_2O) assuming that the molecular interactions between the porphyrin molecules and MCM-41 are comparable.

Table 1. Evaluation of porphyrin loadings inside MCM-41 using UV-Vis spectroscopy.

sample	Soret (nm)	A Soret	(amount per 2 mg) x 10^6 [a]	Q bands (nm)	Solvent[b]
TPP (ε = 519 000 $M^{-1}cm^{-1}$)	417	—	—	515, 549, 569, 646	CH_2Cl_2
TPP@MCM-41 (5 mg)	418	0.219	1.88	—	CH_2Cl_2
TPP@MCM-41 (10 mg)	429	0.221	1.89	—	CH_2Cl_2
TPP@MCM-41 (15 mg)	420	0.227	1.94	—	CH_2Cl_2

TPP@MCM-41 (20 mg)	420	0.245	2.10	–	CH_2Cl_2
ZnTNMPyP (ε = 94 000 $M^{-1}cm^{-1}$)	438	–	–	568, 608	H_2O
ZnTNMPyP@MCM-41 (5 mg)	449	0.410	13.8	571	H_2O
ZnTNMPyP@MCM-41 (10 mg)	455	0.445	14.9	571	H_2O
ZnTNMPyP@MCM-41 (15 mg)	457	0.475	15.8	572	H_2O
ZnTNMPyP@MCM-41 (20 mg)	456	0.662	22.0	573	H_2O
TNMPyP (ε = 239 000 $M^{-1}cm^{-1}$)	421	–	–	518, 551, 585	H_2O
TNMPyP@MCM-41 (5 mg)	431	0.498	7.0	520, 550	H_2O
TCPP (ε = 486 700 $M^{-1}cm^{-1}$)	420	–	–	514, 550, 590, 645	DMSO
TCPP@MCM-41 (5 mg)	420	0.026	<0.01	–	DMSO
ZnTCPP (ε = 267 600 $M^{-1}cm^{-1}$)	422	–	–	558, 596	H_2O
ZnTCPP@MCM-41 (5 mg)	422	0.740	9.1	–	H_2O

a) Amount in mg per 2 mg of MCM-41. b) The choice of solvent is based on the solubility issue of the porphyrin derivatives.

X-Ray Diffraction (XRD)

The powder X-ray diffraction spectra of all porphyrin@MCM-41 materials show similar patterns with MCM-41 (Supplementary Materials). Three reflections at ~2.5° (d_{100}), ~4° (d_{110}), and ~5° (d_{200}), characteristic of the MCM-41 hexagonal structure, are observed in the 2θ range, which means that the structure and arrangement of MCM-41 channels were not affected by the encapsulation of porphyrins. The absence of a crystalline porphyrin peak after encapsulation indicates that porphyrin is well incorporated in the channels of MCM-41 and does not form aggregates. Figure 3a exhibits the structure of MCM-41 and its channels [48], and the incorporation of ZnTCPP inside the pores (docking) shows no steric problems.

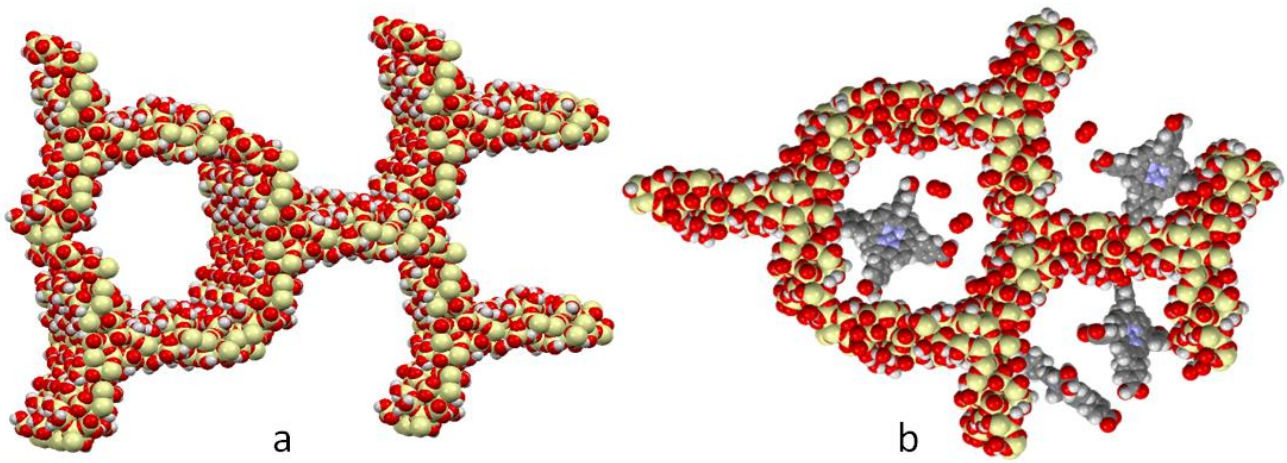

Figure 3. (a) Space-filling structure of MCM-41 according to reference 48 (image built based on a cif file). (b) Proposed space-filling structure of the host-guest composite ZnTCPP@MCM-41 (color code: yellow = silicium, red = oxygen, white = hydrogen, grey = carbon, blue = nitrogen). O_2 molecules have been added to this image to show the relative space available for the gas.

Thermogravimetric Analyses (TGA)

The stability of the composites has been assessed by TGA by comparison with that of MCM-41 (the traces are placed in the Supplementary Materials). The first weight loss of 4% for MCM-41 corresponds to the expected desorption of water below 150°. The next weight losses are observed above 200° for the porphyrin@MCM-41 host-guest composites. These losses correspond to the thermal degradation of organic species (namely porphyrins). These weight losses vary from about 7 to 12% depending on the guest's porphyrin. The highest porphyrin weight loss was noted for TPP@MCM-41 (weight loss = 12%). The amplitude of this weight loss corroborates the BET findings. Moreover, TNMPyP@MCM-41 exhibits the lowest porphyrin weight loss, which was also confirmed by BET analyses below.

Brunauer-Emmett-Teller (BET)

The BET surface area, S_{BET}, of the composites was evaluated using the N_2(g) isotherms at 77K (Figure 4). The data are as follow: TPP@MCM-41 (914 $m^2\,g^{-1}$), TPP@MCM-41 (direct synthesis; 592 $m^2\,g^{-1}$), ZnTNMPyP@MCM-41 (771 $m^2\,g^{-1}$), ZnTCPP@MCM-41 (813 m^2g^{-1}) and TNMPyP@MCM-41 (832 m^2g^{-1}). For comparison purposes, the S_{BET} of MCM-41 is 1690 m^2g^{-1} [49], which corroborates further that MCM-41 in the host-guest composites is indeed loaded. The striking result is the difference between the S_{BET} values of the composites fabricated by insertion ($771 < S_{BET} < 914$ m^2g^{-1}) versus that for TPP@MCM-41 (direct synthesis, blue curve; 592 $m^2\,g^{-1}$). This difference suggests that the pores of the latter composite are more "filled" than the formers, particularly that for TPP@MCM-41 (914 m^2g^{-1}). To verify whether this is indeed the case, the elemental analysis of TPP@MCM-41 (914 m^2g^{-1}) and TPP@MCM-41 (direct synthesis; 592 $m^2\,g^{-1}$) were obtained (Table 2). It is noteworthy that the loadings of porphyrins inside MCM-41 are weak according to Table 1, and that these amounts are found to be at the detection limit of the elemental analysis method, thus reducing the accuracy for several elements, such as nitrogen. Despite this inconvenience, the data indeed confirm the trend; larger loading leads to smaller S_{BET} values.

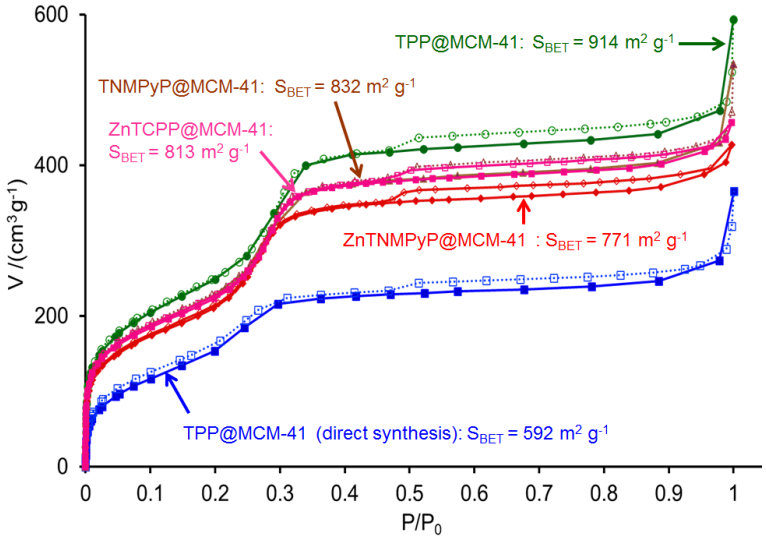

Figure 4. BET isotherms of the host-guest composites of MCM-41.

Table 2. Comparison of the S_{BET} data for the TPP-containing composites.[a]

Host-guest composites	N %	C %	H %	S_{BET} (m^2g^{-1})
TPP@MCM-41 (5 mg)	0.00[b]	2.86	0.85	914
TPP@MCM-41 (20 mg)	0.00[b]	2.80	0.90	—[c]
TPP@MCM-41 (direct reaction)	0.51	11.55	2.09	592

MCM-41 (commercial)	0.00	0.22	1.76[d]	—[c]

a) Note that the N%, C%, and H% are similar for both the 5 mg and 20 mg samples, which is consistent with the data of Table 1 indicating only a modest variation of loading between the two samples. b) Note that for small amounts of porphyrins such as exposed 5 mg and 20 mg translating to 1.88 x 10^6 and 2.10 x 10^6 mg per 2 mg of MCM-41, the data are found to be at the detection limit, so the uncertainties are high. c) Not measured. d) Most likely water as confirmed by IR spectroscopy.

Photophysical studies

Proof of concept

To demonstrate the photosensitization of the selected porphyrins, composite ZnTNMPyP@MCM-41 deposited onto a quartz plate was tested as a representative example (Figure 5). Both the quartz plate and the mesoporous silica MCM-41 showed no emission in the near-IR region. Conversely, when MCM-41 is loaded with ZnTNMPyP, an emission band is observed at ~1270 nm precisely where the $^1O_2(g)$ phosphorescence is expected [50,51]. The excitation spectrum of this band matches that of ZnTNMPyP indicating photosensitization. This direct detection of the $^1O_2(g)$ phosphorescence at the solid state/air interface is rather interesting since the measurements did not require the use of a laser source as is generally the case [52–54]. It is noteworthy that in comparison with an air-saturated solution the need for a laser source stems from the velocity of oxygen in the air (480 m/s at 298K, which corresponds to 0.48 mm/μs). With an emission lifetime of $^1O_2(g)$ ranging from 550 μs [55] to 0.4 s [56] the molecules have enough time to linearly travel (which is obviously not the case in a real situation but still) from 0.26 to 1.92 x 10^4 cm, respectively, before emission. With slits of several millimeters wide, the $^1O_2(g)$ molecules can easily be out of the analytical beam, rendering the observed signal significantly weaker. In brief, the observation of the $^1O_2(g)$ emission reported in the literature is greatly facilitated by the use of high-intensity excitation sources, such as lasers, which is not the case here. The reason for the successful direct observation of the $^1O_2(g)$ emission using a conventional lamp (100W Xe lamp) here stems from the formation of these excited molecules inside the pores where the porphyrin sensitizers stand in the mesoporous material, rendering the escape of $^1O_2(g)$ slower. Concurrently, the weak loading deduced in Table 1 also indicates that the observation of this $^1O_2(g)$ phosphorescence may be more challenging compared to a pure porphyrin sample, thus resulting in a lower signal/noise ratio. No degradation was observed within the timeframe of the measurements.

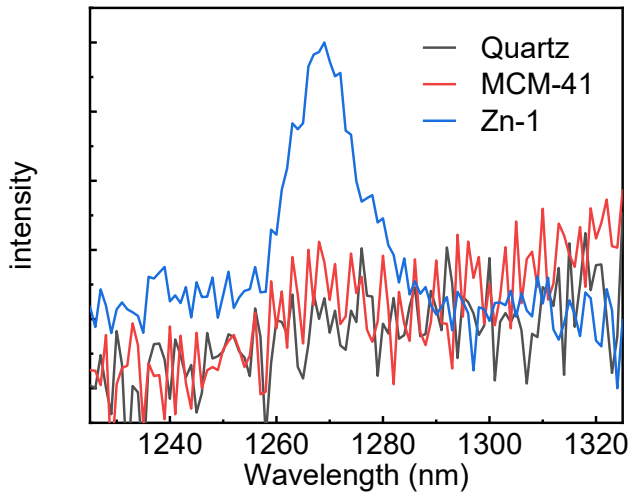

Figure 5. Solid state near-infrared emission of **Zn-1** (ZnTNMPyP@MCM-41; 5 mg), MCM-41 alone, and quartz sample holder (intensity is relative), λ_{exc} = 450 nm.

Analysis of the MCM-41 composites

Figures 6 and 7 display the characteristic profiles for the near-IR emission at the composites' solid state/air interface in the presence of air. Figure 8 shows the instrumental setup for such measurements.

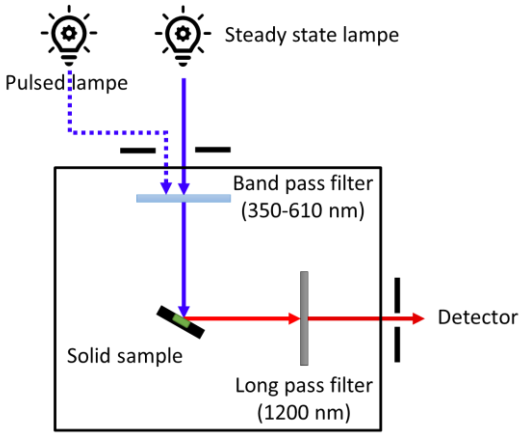

Figure 8. Experimental setup for emission measurement.

The radiative emission decay in solution was monitored at 1275 nm with a similar setup but a Hamamatsu 15 W Xenon Flash Lamp was used as an excitation source. The results were fitted with Origin software with a two-phase exponential decay function with time constant parameter model $\left(I(\lambda,t) = I_0 + A_1\, e^{-\frac{t}{\tau_1}} + A_2\, e^{-\frac{t}{\tau_2}}\right)$.

Interestingly, despite the obvious difference in porphyrin loadings (Table 1), the phosphorescence intensity of $^1O_2$(g) is approximately equal for all samples, including that for TPP@MCM-41 obtained from a direct formation of TPP inside the pores of MCM-41 (labeled H2-5 below). No clear trend was observed for each series of samples. In fact, the relative intensity of the $^1O_2$(g) phosphorescence is found to be within the same order of magnitude. This observation may be due that the loading is primarily higher at the surface of the MCM-41 particles as deduced above.

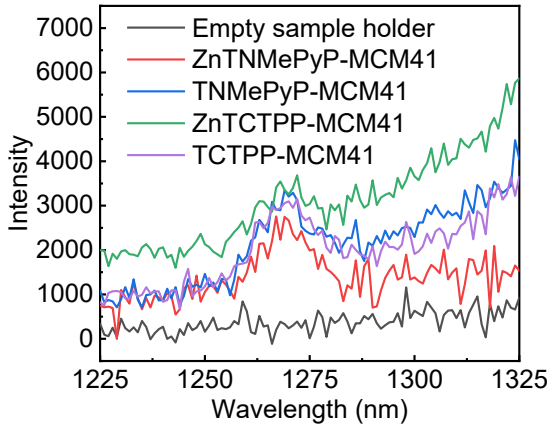

Figure 6. Emission of $^1O_2$(g) at the solid state/air interfaces of composites ZnTNMPyP@MCM-41 (λ_{ex} = 460 nm), TNMPyP@MCM-41 (λ_{ex} = 428 nm), ZnTCPP@MCM-41 (λ_{ex} = 426 nm) and TCPP@MCM-41 (λ_{ex} = 413 nm). All these samples were prepared with the exposition of 5 mg loads.

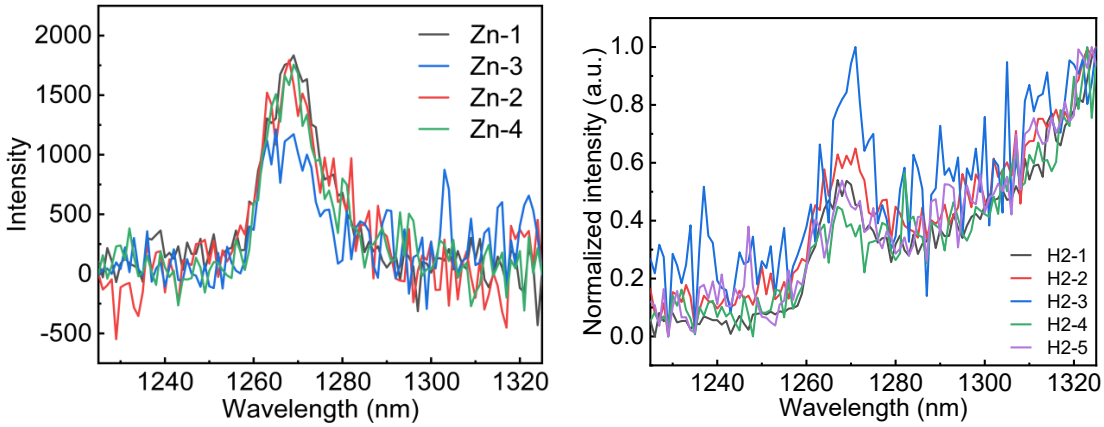

Figure 7. (Left) Near-IR emission of $^1O_2$(g) at the interfaces of ZnTNMPyP@MCM-41 labeled **Zn-1** to **Zn-4**, where **1-4** stands for ZnTNMPyP@MCM-41 (5 mg; 10 mg; 15 mg; and 20 mg), respectively. (Right) Near-IR emission of TPP@MCM-41 labeled **H2-1** to **H2-5**, where **1-4** stands for TPP@MCM-41 (5 mg; 10 mg; 15 mg; and 20 mg, and direct synthesis, respectively. Note that this figure is presented in a normalized intensity scale for aesthetic reasons due to the baseline.

The phosphorescence decay traces of the $^1O_2$(g) at the solid sample/air interfaces were too weak or too short to be accurately measured with the setup available. Any decay times of ~ 20 μs or less fall outside the instrument response (Supporting Information). Instead, the composites were suspended in solution.

Suspension in CH_2Cl_2 and $CHCl_3$

The $^1O_2$ phosphorescence spectra and decay traces of the ZnTNMPyP@MCM-41 and TPP@MCM-41 composites suspended in CH_2Cl_2 and $CHCl_3$ are provided in the Supporting Information. First, a compilation of the $^1O_2$ phosphorescence lifetimes in CH_2Cl_2 and $CHCl_3$ reported in the literature [57–61] indicates that these values are 101 ± 39 μs and 235 ± 30 μs, respectively. For the composites, the decay traces are found to be biexponential (Table 3). The long components are of very weak intensity (pre-exponential factor A_2) and are readily associated with $^1O_2$ dissolved in the solvent by comparison with the literature data. The presence of this weak component may be due to both $^1O_2$ escaping the mesoporous material and the photosensitizer leaching out MCM-41. The decay time of this component, τ_2, is found to be relatively constant for all samples considering the uncertainties.

Table 3. Photophysical parameters of the singlet oxygen in two different environments.

	CH_2Cl_2 suspension[b]				$CHCl_3$ suspension[b]			
Sample[a]	A_1	τ_1 (μs)	A_2	τ_2 (μs)	A_1	τ_1 (μs)	A_2	τ_2 (μs)
Literature[c]	-	-	-	101 ± 39	-	-	-	235 ± 30
Zn-1	485	20 ± 4	0.45	102 ± 10	3.4	27 ± 6	0.18	197 ± 20
Zn-2	8819	14 ± 3	0.08	116 ± 12	1042	17 ± 3	0.03	232 ± 23
Zn-3	33463	12 ± 3	0.03	134 ± 13	2113	16 ± 3	0.02	234 ± 23
Zn-4	25522	12 ± 3	0.03	140 ± 14	2626	15 ± 3	0.02	213 ± 21
H2-1	2.1	65 ± 13	2.5	100 ± 10	377	13 ± 3	1.6	224 ± 23
H2-2[d]	3.2	30 ± 6	3.2	92 ± 10	126594	[8.9]	0.7	225 ± 23
H2-3[d]	-	[8.3]	1.5	89 ± 10	-	[8.0]	0.7	221 ± 22
H2-4[d]	-	[8.5]	2.2	91 ± 10	-	[7.9]	0.7	226 ± 23

a) The ZnTNMPyP@MCM-41 samples are labeled as **Zn-1** to **Zn-4**, where **1-4** stands for ZnTNMPyP@MCM-41 (5 mg; 10 mg; 15 mg; and 20 mg), respectively, and TPP@MCM-41 samples are labeled as **H2-1** to **H 2-5**, where **1-4** stands for TPP@MCM-41 (5 mg; 10 mg; 15 mg; and 20 mg). b) $I_e(t) = A_1 \exp(-t/\tau_1) + A_2 \exp(-t/\tau_2)$. The uncertainties are generally ± 10 % for the long component, and 20 % for the short one. c) Compilation of the reported phosphorescence lifetimes of $^1O_2$ in CH_2Cl_2 and $CHCl_3$; from [57–61]. The uncertainties are defined by the upper and lower limits of the uncertainties reported in this compilation. d) In this case, the decay traces are at the limit of the detection capability of the instrument, consequently the values placed inside square brackets are considered inaccurate.

Concurrently, the time constants of the short-lived components are generally one order of magnitude shorter than that for the long-lived one, except for the case TPP@MCM-41 in CH_2Cl_2. This difference is explained by the different environment of $^1O_2$ inside MCM-41 *versus* dissolved. It is well-known that the phosphorescence lifetime of $^1O_2$ is strongly medium dependent. For example, the emission lifetime of $^1O_2$(g) ranges from 550 μs [55] to 0.4 s [56] depending on the pressure. For $^1O_2$ inside MCM-41, the τ_1 value ranges from 12 to 27 μs. These values are in full agreement with those reported of $^1O_2$ generated inside other silica-based matrices such as microporous silica xerogel (~16 μs) [62] and porous silica monoliths (~25 μs) [63]. Excluding the uncertainties, one finds that $\tau_1(CH_2Cl_2) < \tau_1(CHCl_3)$, which is consistent with the fact that $\tau_2(CH_2Cl_2) < \tau_2(CHCl_3)$ This observation implies that the pores are also filled with solvent molecules as expected (Figure 3b). The main conclusion from these measurements is that $^1O_2$ is

readily produced at both the solid-state/liquid interfaces (which are readily escaping into the solvent) and inside the pores of the mesoporous MCM-41.

The odd series of the data in this investigation is the case TPP@MCM-41 in CH_2Cl_2, which do not follow the observed trends. It is highly suspected that TPP is very soluble in CH_2Cl_2, which was used as the solvent for loading MCM-41, and thus the leaching out process is accentuated in this case. This assumption is supported by the observation of the pre-exponential factors, A_1 and A_2, are nearly equal. Consequently, the extracted short component could be a mixture of short and long components lost in a poor set of data, due to the detection limit of the instrument.

CONCLUSION

New porous composite MCM-41 materials using various porphyrin derivatives as photosensitizers have been prepared and characterized by several techniques. The loading of MCM-41 was achieved by slow diffusion in a given solvent or, in one case, by a direct reaction inside the mesoporous material. UV-Vis, TGA and XRD spectra confirmed not only the successful incorporation of porphyrins but also that structure of hexagonal channels of MCM-41 remains unchanged after porphyrin incorporation. BET analyses showed a decrease in the surface area of complexes and with this demonstrated incorporation of porphyrin in it. These results were also proved by elemental analyses. Altogether, the characterization data strongly suggest that the loading from slow diffusion occurs at the surface of the particles mostly, which is a logical outcome. The production of singlet oxygen was demonstrated by the direct observation of the $^1O_2(g)$ phosphorescence at ~1270 nm at the solid-state/air interface. As such, this detection without the use of a laser source to overcome the fast velocity of $O_2(g)$ escaping the analytical beam, is an achievement. Moreover, the measurements of the phosphorescence lifetimes of $^1O_2$ inside the mesoporous, and consequently confirmation of its presence, have been performed from suspensions of the composites in organic solvents. All in all, the reported mesoporous composites herein are good candidates for performing heterogeneous photocatalytic reactions such as visible-light-driven eradication of toxins and pollutants in water [39], organic transformations [40], formation of solar fuels [41], and more recently, in agriculture as an emerging field [64].

Acknowledgment

The research was supported by the Natural Sciences and Engineering Research Council of Canada, NSERC/CRSNG.

Supporting information

Figures S1–S20 are given in the supplementary material. This material is available free of charge *via* the Internet at http://www.worldscientific.com/doi/suppl/##.####/############

REFERENCES

1. Gong X, Shu Y, Jiang Z, Lu L, Xu X, Wang C and Deng H. *Angew. Chemie - Int. Ed.* 2020; **59**: 5326-5331.
2. Firdaus RM, Desforges A, Rahman Mohamed A and Vigolo B. *J. Clean. Prod.* 2021; **328**: 129553.
3. Lin R-B, Zhang Z and Chen B. *Acc. Chem. Res.* 2021; **54**: 3362-3376.
4. Saini H, Otyepková E, Schneemann A, Zbořil R, Otyepka M, Fischer RA and Jayaramulu K. *J. Mater. Chem. A* 2022; **10**: 2751-2785.
5. Luo H, Gu Y, Liu D and Sun Y. *Catalysts* 2021; **11**: 1557.
6. Yang P, Chen Z, Liu S, Qiao C, Xia Y and Wang Z. *Biomed. Mater.* 2021; **16**: 042011.
7. Fu S, Yao S, Guo S, Guo G-C, Yuan W, Lu T-B and Zhang Z-M. *J. Am. Chem. Soc.* 2021; **143**: 20792-20801.
8. Xin Z, Liu J, Wang X, Shen K, Yuan Z, Chen Y and Lan Y-Q. *ACS Appl. Mater. Interfaces* 2021; **13**: 54959-54966.
9. Hu H, Wang Z, Cao L, Zeng L, Zhang C, Lin W and Wang C. *Nat. Chem.* 2021; **13**: 358-366.
10. Choi S, Jung W-J, Park K, Kim S-Y, Baeg J-O, Kim CH, Son H-J, Pac C and Kang SO. *ACS Appl. Mater. Interfaces* 2021; **13**: 2710-2722.
11. Jin H-G, Chen F, Zhang H, Xu W, Wang Y, Fan J and Chao Z-S. *J. Mater. Sci.* 2020; **55**: 16184-16196.
12. Yu K, Puthiaraj P and Ahn W-S. *Appl. Catal. B Environ.* 2020; **273**: 119059.
13. Zhang C, Yang H, Zhong D, Xu Y, Wang Y, Yuan Q, Liang Z, Wang B, Zhang W, Zheng H, Cheng T and Cao R. *J. Mater. Chem. A* 2020; **8**: 9536-9544.
14. Mayers JM and Larsen RW. *Inorg. Chem. Commun.* 2019; **107**: 107457.
15. Xiao Y, Guo W, Chen H, Li H, Xu X, Wu P, Shen Y, Zheng B, Huo F and Wei WD. *Mater. Chem. Front.* 2019; **3**: 1580-1585.
16. Zhang Z, Zhang L, Wojtas L, Eddaoudi M and Zaworotko MJ. *J. Am. Chem. Soc.* 2012; **134**: 928-933.
17. Larsen RW, Wojtas L, Perman J, Musselman RL, Zaworotko MJ and Vetromile CM. *J. Am. Chem. Soc.* 2011; **133**: 10356-10359.
18. Chen J, Wang Y, Niu H, Wang Y, Wu A, Shu C, Zhu Y, Bian Y and Lin K. *ACS Appl. Mater. Interfaces* 2021; **13**: 45201-45213.

19. Yuan K, Song T, Wang D, Zhang X, Gao X, Zou Y, Dong H, Tang Z and Hu W. *Angew. Chemie Int. Ed.* 2018; **57**: 5708-5713.
20. Ghoochani SH, Heshmati A, Hosseini HA and Darroudi M. *Environ. Sci. Pollut. Res.* 2022; **29**: 34406-34418.
21. Sun T, Zhang X, Hu Y, Xu L and Zhao Y. *Appl. Surf. Sci.* 2022; **572**: 151512.
22. Ren S-Z, Zhu X-H, Wang B, Liu M, Li S-K, Yang Y-S, An H and Zhu H-L. *J. Mater. Chem. B* 2021; **9**: 4678-4689.
23. Gao Y, Lu J, Xia J and Yu G. *ACS Appl. Mater. Interfaces* 2020; **12**: 12706-12716.
24. Liberman I, Shimoni R, Ifraemov R, Rozenberg I, Singh C and Hod I. *J. Am. Chem. Soc.* 2020; **142**: 1933-1940.
25. Wang L, Jin P, Duan S, She H, Huang J and Wang Q. *Sci. Bull.* 2019; **64**: 926-933.
26. Xie Y, Huang Y, Wu C, Yuan W, Xia Y, Liu X and Wang H. *Mol. Catal.* 2018; **452**: 20-27.
27. Hajian R and Ehsanikhah A. *Chem. Phys. Lett.* 2018; **691**: 146-154.
28. Zanardi FB, Barbosa IA, de Sousa Filho PC, Zanatta LD, da Silva DL, Serra OA and Iamamoto Y. *Microporous Mesoporous Mater.* 2016; **219**: 161-171.
29. Silva M, Fernandes A, Bebiano SS, Calvete MJF, Ribeiro MF, Burrows HD and Pereira MM. *Chem. Commun.* 2014; **50**: 6571-6573.
30. Bhattacharyya S, Lelong G and Saboungi M-L. *J. Exp. Nanosci.* 2006; **1**: 375-395.
31. Uthappa UT, Brahmkhatri V, Sriram G, Jung H-Y, Yu J, Kurkuri N, Aminabhavi TM, Altalhi T, Neelgund GM and Kurkuri MD. *J. Control. Release* 2018; **281**: 70-83.
32. Idris SA, Harvey SR and Gibson LT. *J. Hazard. Mater.* 2011; **193**: 171-176.
33. Haddoum S, Fechete I, Donnio B, Garin F, Lutic D and Chitour CE. *Catal. Commun.* 2012; **27**: 141-147.
34. Fechete I, Donnio B, Ersen O, Dintzer T, Djeddi A and Garin F. *Appl. Surf. Sci.* 2011; **257**: 2791-2800.
35. Yu H, Zhang H, Yang W, Feng J, Fan W and Song S. *Microporous Mesoporous Mater.* 2013; **170**: 113-122.
36. Beck JS, Vartuli JC, Roth WJ, Leonowicz ME, Kresge CT, Schmitt KD, Chu CTW, Olson DH, Sheppard EW, McCullen SB, Higgins JB and Schlenker JL. *J. Am. Chem. Soc.* 1992; **114**: 10834-10843.
37. Harvey PD and Plé J. *J. Inorg. Organomet. Polym. Mater.* 2021; **31**: 2715-2756.
38. Schlachter A, Asselin P and Harvey PD. *ACS Appl. Mater. Interfaces* 2021; **13**: 26651-26672.
39. Harvey PD. *J. Porphyr. Phthalocyanines* 2021; **25**: 583-604.
40. Harvey PD. *J. Mater. Chem. C* 2021; **9**: 16885-16910.
41. Asselin P and Harvey PD. *ACS Appl. Nano Mater.* 2022; **5**: 6055-6082.
42. Silva M, Azenha ME, Pereira MM, Burrows HD, Sarakha M, Forano C, Ribeiro MF and Fernandes A. *Appl. Catal. B Environ.* 2010; **100**: 1-9.
43. Silva M, Azenha ME, Pereira MM, Burrows HD, Sarakha M, Ribeiro MF, Fernandes A, Monsanto P and Castanheira F. *Pure Appl. Chem.* 2009; **81**: 2025-2033.
44. Molinari A, Maldotti A, Bratovcic A and Magnacca G. *Catal. Today* 2011; **161**: 64-69.
45. Faraon V and Ion RM. *Optoelectron. Adv. Mater. - Rapid Commun.* 2020; **4**: 1135-1140.
46. Adler AD, Longo FR and Shergalis W. *J. Am. Chem. Soc.* 1964; **86**: 3145-3149.
47. Kalyanasundaram K. *Inorg. Chem.* 1984; **23**: 2453-2459.
48. Ugliengo P, Sodupe M, Musso F, Bush IJ, Orlando R and Dovesi R. *Adv. Mater.* 2008; **20**: 4579-4583.
49. Jang CR, Matei V, Borcea A, Voicu V, Proscanu R and Ciuparu D. *Analele Univ. 'Ovidius' Constanta - Ser. Chim.* 2012; **23**: 133-136.
50. Kumasaka R, Kikuchi A and Yagi M. *Photochem. Photobiol.* March 2014: n/a-n/a.
51. Hu W, Zhang R, Zhang X-F, Liu J and Luo L. *Spectrochim. Acta Part A Mol. Biomol. Spectrosc.* 2022; **272**: 120965.
52. Cantau C, Pigot T, Manoj N, Oliveros E and Lacombe S. *ChemPhysChem* 2007; **8**: 2344-2353.
53. Howells SC, Black G and Schlie LA. *Synth. Met.* 1994; **62**: 1-7.
54. Khalil GE, Chang A, Gouterman M, Callis JB, Dalton LR, Turro NJ and Jockusch S. *Rev. Sci. Instrum.* 2005; **76**: 054101.
55. Durantini AM and Greer A. *Environ. Sci. Technol.* 2021; **55**: 3559-3567.
56. Ruzzi M, Sartori E, Moscatelli A, Khudyakov I V. and Turro NJ. *J. Phys. Chem. A* 2013; **117**: 5232-5240.
57. Boix-Garriga E, Rodríguez-Amigo B, Planas O and Nonell S. In Singlet Oxygen. , 2016; 23-46.
58. Wilkinson F and Brummer JG. *J. Phys. Chem. Ref. Data* 1981; **10**: 809-999.
59. Wilkinson F, Helman WP and Ross AB. *J. Phys. Chem. Ref. Data* 1995; **24**: 663-677.
60. Schweitzer C and Schmidt R. *Chem. Rev.* 2003; **103**: 1685-1758.
61. Hurst JR, McDonald JD and Schuster GB. *J. Am. Chem. Soc.* 1982; **104**: 2065-2067.
62. Cantau C, Pigot T, Manoj N, Oliveros E and Lacombe S. *ChemPhysChem* 2007; **8**: 2344-2353.
63. Lacombe S, Soumillion J-P, El Kadib A, Pigot T, Blanc S, Brown R, Oliveros E, Cantau C and Saint-Cricq P. *Langmuir* 2009; **25**: 11168-11179.
64. Sajjadinezhad SM, Tanner K and Harvey PD. *J. Mater. Chem. B* 2022; **10**: 9054-9080.